ACS SENSORS

pubs.acs.org/acssensors Article

Plant Virus Sensor for the Rapid Detection of Bean Pod Mottle Virus Using Virus-Specific Nanocavities

Nawab Singh, Raufur Rahman Khan, Weihui Xu, Steven A. Whitham, and Liang Dong*

Cite This: https://doi.org/10.1021/acssensors.3c01478 Read Online

ACCESS | Metrics & More | Article Recommendations | Supporting Information

ABSTRACT: This study presents a miniaturized sensor for rapid, selective, and sensitive detection of bean pod mottle virus (BPMV) in soybean plants. The sensor employs molecularly imprinted polymer technology to generate BPMV-specific nanocavities in porous polypyrrole. Leveraging the porous structure, high surface reactivity, and electron transfer properties of polypyrrole, the sensor achieves a sensitivity of 143 μA ng^{-1} mL cm^{-2}, a concentration range of 0.01−100,000 ng/mL, a detection time of less than 2 min, and a detection limit of 41 pg/mL. These capabilities outperform those of conventional methods, such as enzyme-linked immunosorbent assays and reverse transcription polymerase chain reactions. The sensor possesses the ability to distinguish BPMV-infected soybean plants from noninfected ones while rapidly quantifying virus levels. Moreover, it can reveal the spatial distribution of virus concentration across distinct leaves, a capability not previously attained by cost-effective sensors for such detailed viral data within a plant. The BPMV-specific nanocavities can also be easily restored and reactivated for multiple uses through a simple wash with acetic acid. While MIP-based sensors for plant virus detection have been relatively understudied, our findings demonstrate their potential as portable, on-site diagnostic tools that avoid complex and time-consuming sample preparation procedures. This advancement addresses a critical need in plant virology, enhancing the detection and management of plant viral diseases.

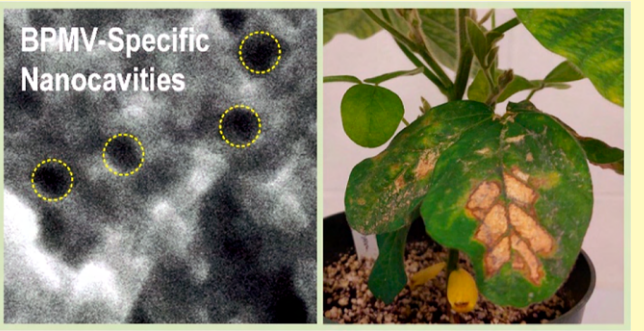

KEYWORDS: *plant sensor, agricultural sensor, virus detection, bean pod mottle virus, molecularly imprinted polymer*

The global food crisis is a significant challenge due to rapid population growth, limited agricultural land, and climate change.[1] Plant disease outbreaks are increasing and have a significant impact on food security worldwide. Biotic factors (e.g., viruses, bacteria, fungi, and insects) coupled with abiotic factors (e.g., temperature and moisture extremes, nutrient deficiencies, and chemicals) are the causal agents of these outbreaks.[2−4] Diseases caused by plant viruses are among the major biotic factors that cause significant economic loss. Soybean production can be significantly affected by several viruses, including bean pod mottle virus (BPMV).[5] BPMV is a member of the genus *Comovirus*, and it has a bipartite, positive-strand RNA genome.[6−9] The genomic RNAs are packaged in nonenveloped, icosahedral virions that are about 28 nm in diameter.[6] BPMV is a significant threat to soybean yield and seed quality[8,10−17] due to its ability to delay maturation and induce green stem, mottling on the leaves, and seed coat mottling.[7,9−12] The mixed infection of BPMV and soybean mosaic virus (SMV) can reduce yield by up to 85%, resulting in substantial economic losses.[7,12] BPMV is transmitted in soybean fields by leaf-feeding beetles, which can easily move from one plant to another and have relatively long distances from field to field. Rapid, accurate, and on-site detection of BPMV infection would provide the information needed to implement appropriate disease management measures to prevent further spread of BPMV.

The detection of BPMV conventionally involves an enzyme-linked immunosorbent assay (ELISA) or reverse transcription polymerase chain reaction (RT-PCR).[18−22] While ELISA provides a robust method, its sensitivity may not be sufficient to detect viruses in soybean leaves during early infection. On the other hand, RT-PCR is specific and sensitive but requires RNA purification, the synthesis of complementary DNA, and PCR using virus-specific oligonucleotide primers. Both of these diagnostic methods are relatively expensive, time-consuming, consume considerable amounts of reagents, and require bulky and costly equipment; therefore, they are unsuitable for on-site virus detection.[23] Recently, several electrochemical biosensors have been developed for virus monitoring, including citrus tristeza virus,[4] cucumber mosaic virus,[24] and tobacco mosaic

Received: July 18, 2023
Accepted: September 13, 2023

https://doi.org/10.1021/acssensors.3c01478
ACS Sens. XXXX, XXX, XXX−XXX

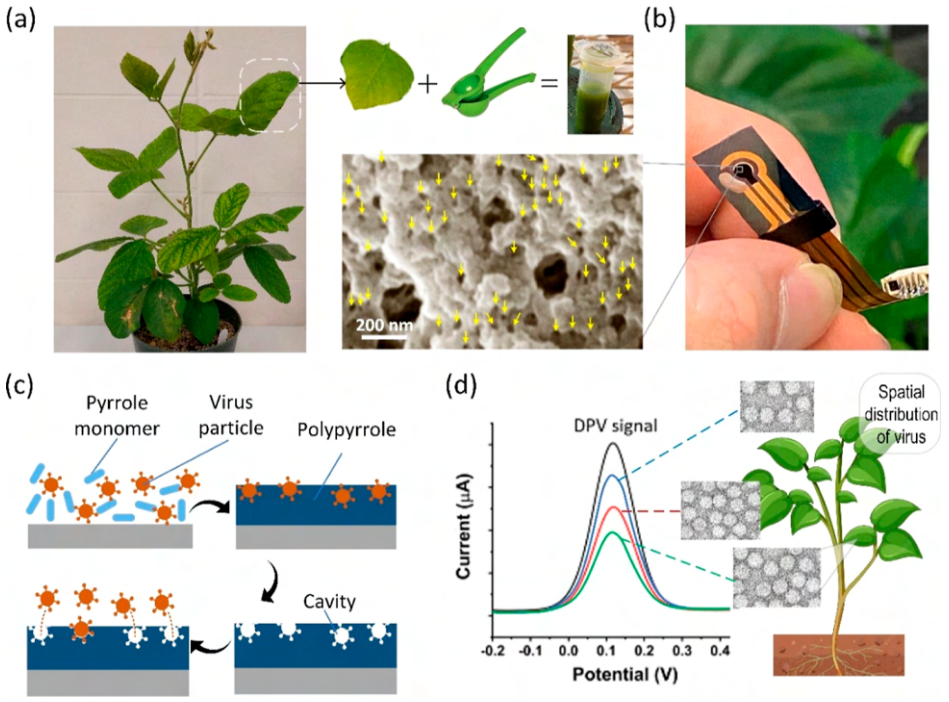

Figure 1. (a) Soybean plant infected with BPMV, illustrating liquid sample extraction from a leaf using a juice squeezer for virus testing. (b) Ppy-based electrochemical sensor fabricated with BPMV-specific nanocavities on the working electrode. A scanning electron microscope (SEM) image shows the electrode surface with small holes marked by yellow arrows indicating the BPMV-targeted nanocavities. (c) Schematic of the MIP synthesis process. (d) Schematic representation highlighting the capacity of the sensor to quantify BPMV concentration distribution across leaves at varying heights of the soybean plant by monitoring the DPV responses to liquid samples obtained from these leaves.

virus.[25] These biomarker-based sensors exhibit high detection performance and portability. However, there is still significant room for improving their sensitivity, selectivity, and shelf life, as well as eliminating the need for low-temperature storage.

With recent advances in nanomaterials and assay strategies, molecularly imprinted polymers (MIPs) have become popular synthetic receptors for detecting biomolecules such as SARS-CoV-2 spike protein,[26] nucleoprotein,[27] troponin,[28] prostate-specific antigen,[29] carcinoembryonic antigen,[30] and viral particles.[31−34] Generally, to form MIPs, template molecules are first trapped in a polymer matrix during monomer polymerization. The template molecules are subsequently removed to create nanocavities complementary in shape and size, which enable specific binding with the target molecules.[26,35] To realize MIP-based biosensors, several transducers have been incorporated, and among these, electrochemical transducers are advantageous over others due to their excellent sensitivity, low cost, high portability, and easy integration with nanomaterials.[36−40] Several electroactive functional monomers have been used for the fabrication of conducting MIPs via electropolymerization. Examples include *m*-phenylenediamine,[41] o-phenylenediamine,[42] aniline,[43] 3,4-ethylenedioxythiophene,[44] and pyrrole.[45] Because of their high conductivity, thermal and chemical stability, and electroactivity,[45,46] these conducting polymers are promising candidates for developing electrochemical MIP-based sensors.

This research presents an electrochemical biosensor designed for the early detection of BPMV in soybean leaves, eliminating the need for additional sample processing steps. It requires only the squeezing of the leaves to obtain test samples (Figure 1a). The sensor effectively recognizes and measures the target virus by utilizing BPMV-specific nanocavities created within the matrix of conducting porous polypyrrole (Ppy) at the surface of an electrochemical transducer by using the MIP technique (Figure 1b,c). The Ppy-based MIP demonstrates high analytical affinity and selectivity for BPMV detection. The sensor offers significant reproducibility, rapid response time, and a wide dynamic range. It effectively distinguishes BPMV-infected soybean plants from noninfected ones and rapidly determines virus concentrations present in simple preparations of leaf sap. Although Ppy-based MIPs have been used to detect substances such as the SARS-CoV-2 virus spike glycoprotein[47] and the carcinogenic amaranth,[48] the development of MIP-based sensors for detecting plant viruses has received limited attention. This study demonstrates the feasibility of creating BPMV-specific nanocavities in Ppy and their effectiveness in detecting BPMV in soybean plants. The validation of this sensor technology gives the sensor the potential to be a portable and on-site diagnostic tool for accurately identifying and monitoring plant virus infections. By focusing on this previously under-researched application, our work addresses a critical need in plant virology and advances the detection and management of plant virus infections. Furthermore, our sensor elucidates the spatial distribution of virus concentration across different leaves of the plant (Figure 1d). Until now, there have been no portable, cost-effective sensors capable of providing such spatial data about viruses within a plant.

EXPERIMENTAL SECTION

Chemicals. All chemicals used were analytical grade, and deionized (DI) water (18.6 MΩ) was used in all experiments. Hydrofluoric acid (HF) and gold (Au) etchants were procured from Fischer Scientific (Waltham, MA, USA). Pyrrole and hydrochloric acid were purchased from Sigma-Aldrich (St. Louis, MO, USA). Phosphate-buffered saline (PBS; 10 mM) was prepared using sodium

https://doi.org/10.1021/acssensors.3c01478
ACS Sens. XXXX, XXX, XXX−XXX

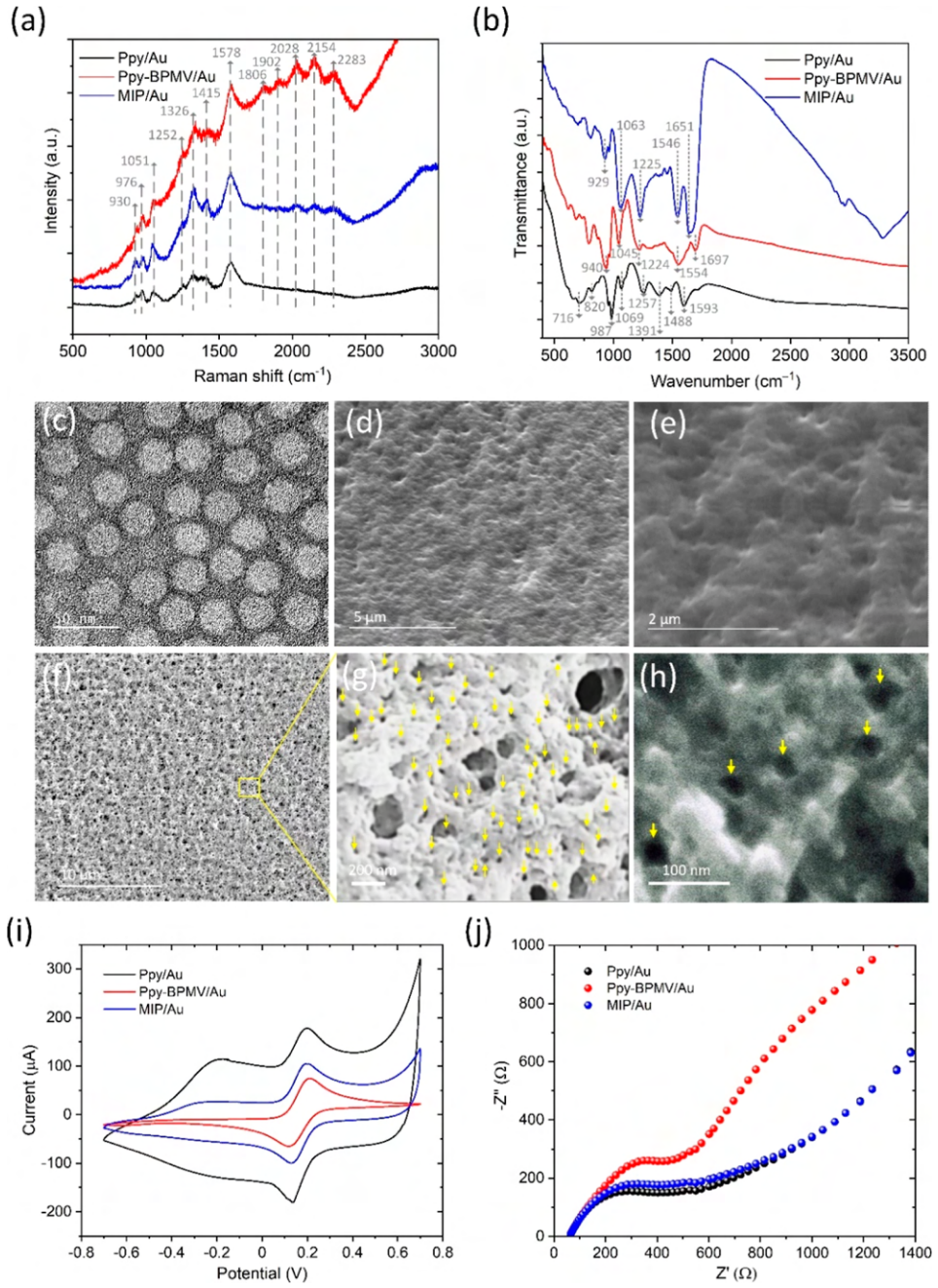

Figure 2. (a,b) Raman (a) and FTIR (b) spectra obtained from the electropolymerized Ppy, Ppy-BPMV, and MIP synthesized on an Au electrode. (**c−h**) Electron microscopy images showing the steps of MIP sensor fabrication. Transmission electron microscopy image of purified BPMV virions used for sensor fabrication (c). SEM images of the electropolymerized Ppy film (d), electropolymerized Ppy-BPMV composite (e), MIP following BPMV removal (f), and close-up image of the nanocavities formed at the surface of Ppy (g,h). The arrows in parts (g,h) point to the nanocavities. (**i,j**) Electrochemical characterization of electropolymerized Ppy, Ppy-BPMV, and MIP on an Au electrode surface, as probed by CV (i) and EIS (j).

dihydrogen phosphate (NaH_2PO_4) and sodium monohydrate phosphate (Na_2HPO_4) (Sigma-Aldrich).

BPMV Purification for Biosensor Fabrication and Testing. The primary leaves from young soybeans were inoculated with BPMV. Leaves displaying strong mosaic disease symptoms were harvested 3−4 weeks after the inoculation. All chemicals used for BPMV purification were purchased from Thermo Fisher (Pittsburgh, PA, USA). Approximately 100 g of leaves were homogenized in ice-cold 0.1 M sodium phosphate buffer [pH 7.0, 1:2.5 (W/V)] containing 0.01 M sodium diethyldithiocarbamate and 0.02 M sodium thioglycolate. The homogenate was filtered through two layers of cheesecloth. The filtrate was homogenized with an equal volume of chloroform/*N*-butanol (1:1, V/V). The homogenate was centrifuged at 15,000*g* for 20 min at 4 °C. The aqueous phase was centrifuged at 85,000*g* for 2.5 h at 4 °C. The pellet was resuspended in 0.1 M sodium phosphate buffer and shaken at 4 °C overnight, followed by centrifugation at 12,000*g* for 10 min at 4 °C. The supernatant was centrifuged at 144,000*g* for 1 h at 4 °C, and the pellet was resuspended in 0.1 M sodium phosphate buffer and shaken for 0.5 h at 4 °C, followed by centrifuging at 12,000*g* for 10 min at 4 °C. The supernatant was then layered on top of a 10−40% sucrose gradient prepared in 0.1 M sodium phosphate buffer and centrifuged for 2.5 h at 100,000*g* at 4 °C. The virus band was visualized with a PGF ip Piston Gradient Fractionator (BioComp Instruments,

https://doi.org/10.1021/acssensors.3c01478
ACS Sens. XXXX, XXX, XXX−XXX

Fredericton, NB E3B 1P6, Canada). The virus sample was collected with a syringe and diluted with 0.1 M sodium phosphate buffer (1:1, V/V). The purified virus particles were pelleted at 144,000 g overnight at 4 °C. Different concentrations of the BPMV viral samples (0.01−100,000 ng/mL) were prepared in PBS (10 mM, pH 7.4) containing 5 mM ferro-ferricyanide from the stock BPMV viral sample (2 mg/mL).

For the preparation of soybean leaf samples (noninfected and BPMV-infected soybean plants), approximately 2 g of soybean leaf tissue was mixed with 2 mL of PBS (10 mM, pH 7.4). The liquid sample was then extracted with a kitchen juice squeezer. The extracted sample, around 25−30 μL of leaf juice, was mixed with 75 μL of PBS (10 mM, pH 7.4), and then this sample was serially diluted from 1×−20× in PBS solution containing 5 mM potassium ferro-ferricyanide.

Device Fabrication. The fabrication process for the BPMV sensor began with forming three thin-film Au electrodes on a silicon wafer with a 100 nm-thick thermal oxide layer. Here, a 150 nm-thick Au layer was deposited using e-beam evaporation. The Au electrodes were then patterned using ultraviolet photolithography and selective etching with a Au etchant solution (GE-8148; Transene; Danvers, MA, UA). The circular working electrode (WE) had a diameter of 3 mm and was surrounded by a counter electrode (CE) and a reference electrode (RE). Next, a 200 μm-thick layer of Ag/AgCl paste (E2414 AG/AGCL Ink, Ercon, USA) was applied to the RE area, followed by thermal treatment on a hot plate at 85 °C for 90 min. For forming the BPMV-specific MIP on the surface of the WE, 30 μL of PBS solution (10 mM; pH 5.0) containing 0.1 molar HCl, 0.1 molar pyrrole, and 2 mg/mL of BPMV particles were applied on the Au electrodes. Subsequently, the electropolymerization of pyrrole was carried out on the Au electrode by the chronoamperometric technique at 0.75 V for 120 s. The optimal electropolymerization time was determined based on the point at which the current level reached saturation during the polymerization process. Figure S1 demonstrates that the polymerization current approached near saturation at 120 s. During the polymerization of pyrrole to Ppy, the BPMV particles were entrapped in the polymer structure. Then, the Ppy surface was washed with PBS and DI water to remove nonpolymerized pyrrole, and then it was rinsed and stirred in 5% acetic acid solution for 20 min at 50 °C to remove the entrapped BPMV particles from the Ppy. Finally, the sensor with the BPMV-specific MIP was washed with DI water and stored at room temperature. In addition, a control device was prepared using the same fabrication method as the sensor, except that no BPMV particles were added to the pyrrole monomer solution for electropolymerization. The control device was used to examine the effectiveness of the nanocavities in MIP for recognizing the target BPMV particles.

Measurement Procedures. In the measurement process, the extracted liquid samples (noninfected and BPMV-infected soybean plants) were serially diluted from 1×−20× fold in a PBS solution containing 5 mM potassium ferro-ferricyanide. The prepared, diluted 30 μL samples were then sequentially pipetted onto the sensor surface. Electrochemical signals were recorded using differential pulse voltammetry (DPV; CHI electrochemical workstation, CHI760E; USA). After the measurement, the sensor was washed with 1% acetic acid, followed by washing in PBS (10 mM, pH 7.4) to regenerate the sensor surface.

Reverse-Transcriptase PCR (RT-PCR). For RT-PCR detection of BPMV, the total RNA was extracted with TRIzol Reagent (Ambion by Life Technologies, Carlsbad, CA). The first-strand cDNA was synthesized using the Maxima First Strand cDNA Synthesis Kit with dsDNase (Thermo Scientific, Coon Rapids, MN), according to the manufacturer's instructions. The synthesized cDNA was used as a template for RT-PCR. BPMV amplicons were amplified using the oligonucleotide primer pairs MCS-1037F (5′-GATCCCCAATACAATGAGG-3′) and MCS-1033R (5′-ATAGACAGAGCATACTCAACG-3′) (1846 bp). Soybean actin (GmActin) was used as the internal control for cDNA integrity, and the GmActin amplicon was amplified by primer pairs GmActinF (5′-CAGGCTGTCTTGTCTCTGTATG-3′) and GmActinR (5′-CTGGGTGCAAGAGCACTAAT-3′) (560 bp). The amplicons were detected using agarose gel electrophoresis combined with a SYBR-Safe DNA Gel Stain (Invitrogen by Thermo Fisher Scientific, Carlsbad, CA).

RESULTS AND DISCUSSION

Material Characterization. Raman studies were conducted to characterize the molecular structure and interactions of electropolymerized Ppy and Ppy-BPMV (Figure 2a). In the Raman spectrum of Ppy, the band found at 1578 cm^{-1} is assigned to C−C stretching. The bands at 1414.5 and 1326 cm^{-1} are related to the C−C and C−N stretching of Ppy, respectively, whereas the band seen at 1252 cm^{-1} is attributed to the C−H in-plane bending.[49,50] The C−H in-plane bending and the ring deformation related to dications are at 1051 and 930 cm^{-1}, while the band at 976 cm^{-1} is associated with radical cations.[49] Thus, in all events, both the dications and radical cations contribute to the conductivity of the electropolymerized Ppy. The Raman spectrum of the electropolymerized Ppy-BPMV shows that in addition to the bands of Ppy, there exist additional bands at 1806, 1902, 2028, and 2154, 2283 cm^{-1} associated with the BPMV particles entrapped into the polymer.[51,52] The increasing intensity at these bands may be due to the presence of imprinted BPMV particles in the Ppy. After the removal of the BPMV particles from Ppy to form MIP, the additional bands of BPMV almost disappeared, further indicating that the BPMV particles were successfully imprinted into the polymer matrix through the electropolymerization process.

Fourier-transform infrared spectroscopy (FTIR) studies were carried out to examine the electropolymerization and functionality of Ppy-BPMV in the MIP (Figure 2b). In the FTIR spectra of Ppy, the peaks at 987 and 1069 cm^{-1} are related to C−O stretching, the peaks at 1257 and 1391 cm^{-1} belong to C−H in-plane vibration, while the peak at 1488 cm^{-1} corresponds to the C−N stretching vibration. The peak at 1593 cm^{-1} relates to C═C stretching vibrations of Ppy [49, 50]. The FTIR spectra of the electropolymerized Ppy-BPMV demonstrate the presence of additional peaks at 1697 and 1554 cm^{-1}, alongside the characteristic peaks of Ppy. These additional peaks can be attributed to the entrapment of BPMV particles within the Ppy structure and are associated with the amide I and II bands, which are indicative of the protein structures found in the virus.[53] Also, several peaks are present in the Ppy-BPMV spectra, but these peaks have shifted to lower wavenumbers. After the removal of the BPMV particles from Ppy, the additional peaks related to BPMV particles disappeared, indicating that the BPMV particles were imprinted into the Ppy matrix.

SEM studies were conducted to characterize the morphology of the fabricated electrodes, including Ppy/Au, Ppy-BPMV/Au, and MIP/Au. Figure 2c shows that the non-enveloped BPMV particles have an icosahedral shape that is about 28 nm in diameter. The surface morphology of Ppy (Figure 2d) is similar to that of Ppy-BPMV (Figure 2e) because the same monomer, Ppy, and procedure were applied during the electropolymerization of these two materials. After the removal of the BPMV particles from the Ppy-BPMV layer, the surface morphology of MIP shows a dramatic change with the formation of nanocavities and porosity (Figure 2f). In Figure 2g,h, tiny holes are observed on the surface of Ppy. The holes, ranging between 25 and 35 nm, align closely with the dimensions of the BPMV particles. This suggests that these

https://doi.org/10.1021/acssensors.3c01478
ACS Sens. XXXX, XXX, XXX−XXX

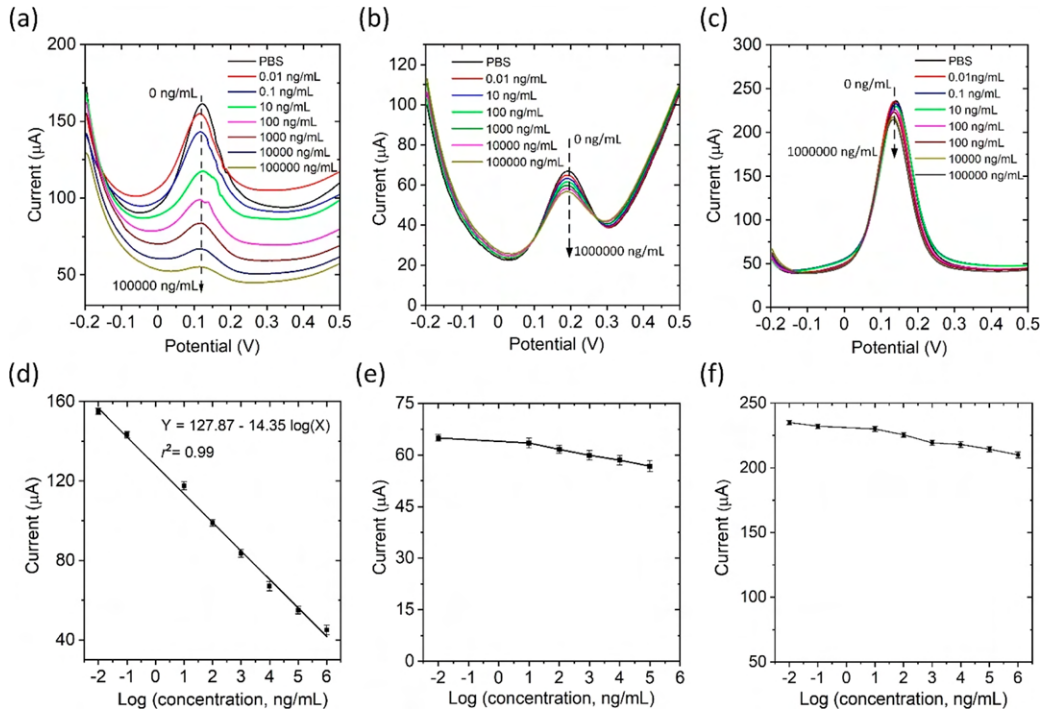

Figure 3. **(a−c)** DPV response of the sensor with the MIP/Au electrode (a), Type-1 control device featuring Ppy-BPMV/Au electrode (b), and Type-2 control device with nonimprinted Ppy/Au electrode (c) when exposed to various concentrations of BPMV (0.01−100,000 ng/mL) in a 10 mM PBS solution (pH7.4) containing 5 mM ferro-ferricyanide. **(d−f)** Calibration curves for the sensor (d), Type-1 control device (e), and Type-2 control device (f) illustrate the relationship between the logarithm of BPMV concentration and DPV peak current.

tiny holes were created following the removal of the BPMV particle templates.

Electrochemical Characterization. Cyclic voltammetry (CV) and electrochemical impedance spectroscopy (EIS) were used to examine the electrochemical behavior of the Ppy/Au, Ppy-BPMV/Au, and MIP/Au electrodes in PBS (10 mM, pH 7.4) containing 5 mM ferro-ferricyanide (Figure 2i,j). The Ppy/Au electrode showed an anodic peak current I_{pa} of 178.3 μA and a cathodic peak current I_{pc} of −180.2 μA at a scan rate of 40 mV s^{-1} (Figure 2i). When the template BPMV particles were entrapped in the Ppy matrix, there was a reduction in the redox peak current of the Ppy-BPMV/Au electrode to I_{pa} = 74.1 μA and I_{pc} = −68.3 μA; this decline may be attributed to the insulating property of the BPMV particles, which impede electron transport from the Ppy to the Au electrode, leading to a decrease in electrochemical current. After the template virus particles were removed, the redox peak currents were found to increase to I_{pa} = 105.5 μA and I_{pc} = −101.1 μA due to the formation of nanocavities in the MIP. The porous MIP provided numerous passages for the ferro-ferricyanide redox probe to reach the Au surface, and there were no insulating virus particles in the MIP. As a result, the redox peak currents of the MIP/Au electrode increased in comparison with those of the Ppy-BPMV/Au electrode. However, the MIP/Au electrode exhibited lower redox peak currents than the Ppy/Au because, compared to the MIP, the Ppy had higher conductivity that could facilitate electron transport through the polymer to the Au electrode. Figure 2j shows the charge transfer resistances (R_{ct}) of the Ppy/Au, Ppy-BPMV/Au, and MIP/Au electrodes based on the EIS measurement. The Ppy/Au had an R_{ct} value of 495 Ω. When Ppy was imprinted with template BPMV particles, the Ppy-BPMV/Au electrode presented an increased R_{ct} value of 681.6 Ω. After the removal of the BPMV particles, the R_{ct} of the MIP/Au electrode decreased to 596 Ω. Therefore, the electrodes with lower R_{ct} values presented higher peak redox currents.

Analytical Performance. Figure 3a displays the DPV response of the sensor to different concentrations of BPMV in PBS (10 mM, pH 7.4) containing 5 mM ferro-ferricyanide. As the BPMV concentration increased to 100,000 ng/mL, the DPV peak current of the sensor notably decreased. This is likely due to the BPMV particles in the sample binding with the nanocavities in the MIP. Given the insulating properties of the BPMV particles, there was a subsequent decrease in the diffusion of electrolytes and electron transport through the Ppy, which resulted in a decline in the DPV current.[26] The calibration plot of the sensor (Figure 3d) demonstrates that the DPV peak current has a linear relationship with the logarithmic concentration of BPMV, which can be described by the equation below

$$I\ (\mu A) = 127.87\ (\mu A) - 14.35\ (\mu A) \times \mathrm{BPMV}\left(\frac{\mathrm{ng}}{\mathrm{mL}}\right),\quad r^2 = 0.996 \qquad (1)$$

The limit of detection (LOD) of the sensor was determined to be 41 pg/mL by using the equation LOD = 3 × SD/m, where SD is the standard deviation of the DPV peak current for the blank solution from three repeated measurements, and m is the slope of the calibration curve. The limit of quantification (LOQ) was determined to be 137 pg/mL using the formula 10 × SD/m.[54]

To illustrate the effect of the nanocavities on the ability of the sensor to recognize and quantify the target BPMV, the first type of control device (namely, Type-1) was formed with the Ppy-BPMV/Au electrode, where the BPMV particles were retained in the matrix of Ppy, and thus, no cavities were

https://doi.org/10.1021/acssensors.3c01478
ACS Sens. XXXX, XXX, XXX−XXX

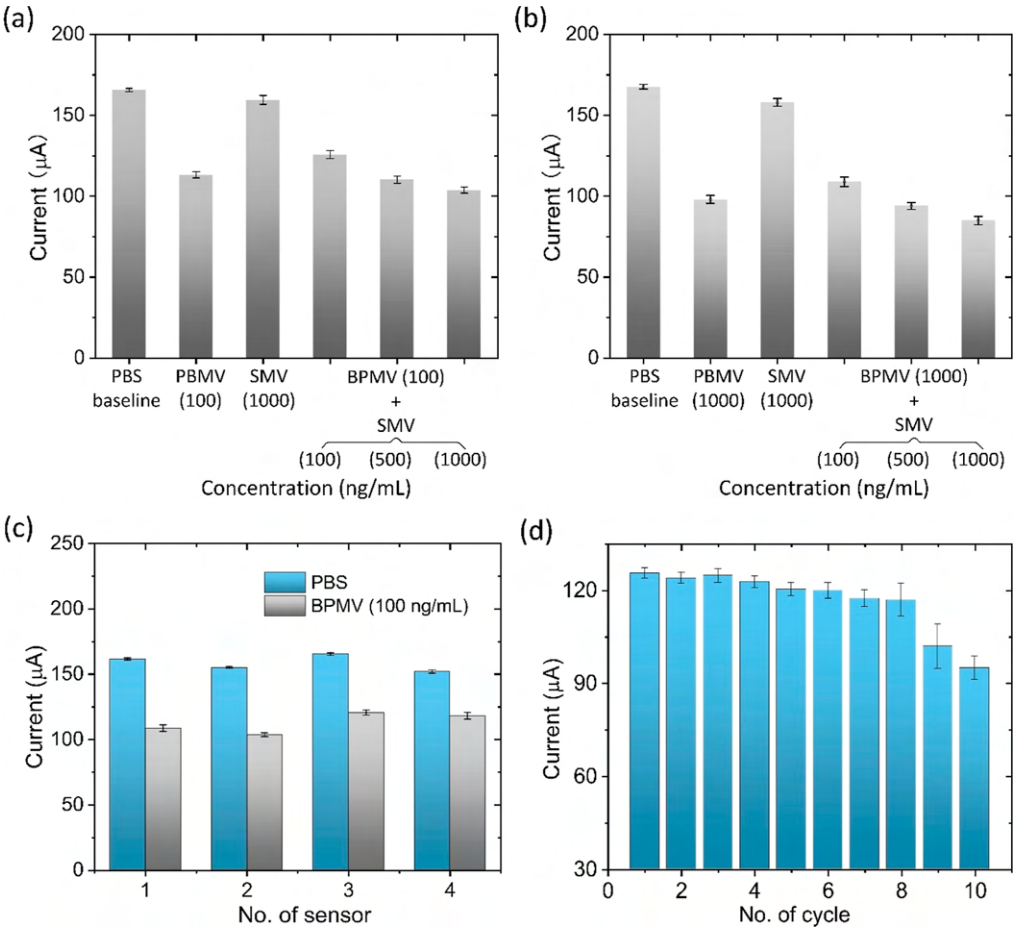

Figure 4. (a,b) Histogram plots illustrating the selectivity of the sensor in the presence of an SMV interferent (100, 500, or 1000 ng/mL) mixed with 100 ng/mL BPMV (a) and 1000 ng/mL BPMV (b). (c) DPV responses of four identical sensors to 100 ng/mL BPMV and PBS solution. (d) Regeneration of BPMV-specific nanocavities in Ppy for BPMV detection. Histogram plot showing the DPV current response of the sensor over successive cycles. Each cycle includes a simple rinsing step using acetic acid and DI water, followed by exposing the sensor to a 50 ng/mL concentration of the BPMV sample.

available in the polymer. The DPV response of this control device to different concentrations of BPMV was examined (Figure 3b). The BPMV samples used here were prepared with PBS (10 Mm, pH 7.4) containing 5 mM ferro-ferricyanide. The DPV response to an increase in concentration of BPMV from 0.01 to 100,000 ng/mL was found to be minimal, with a relative standard deviation (RSD) of 7.9% for the peak current with respect to the baseline (Figure 3e). Furthermore, the other type of control device (Type-2) was formed using the Ppy/Au electrode, which neither created nanocavities nor embedded BPMV particles. Figure 3c shows the DPV response of the Type-2 control device to different concentrations of BPMV in a wide range from 0.01 to 100,000 ng/mL. The DPV peak current was found to only decrease by 8.97% as the concentration of BPMV particles increased by 8 orders of magnitude (Figure 3f); this was attributed mainly to the lack of BPMV-specific nanocavities in the Ppy and partially to the nonporous feature of the Ppy (Figure 2d) that made it hard for the ferro-ferricyanide redox probe to access the Au surface.

The specificity of the sensor in the presence of a combination of BPMV (100 or 1000 ng/mL) and SMV interferent (100, 500, or 1000 ng/mL) is demonstrated in Figure 4a and b. The baseline DPV peak current of the sensor was 166 μA when exposed to 10 mM PBS (pH 7.4) containing 5 mM ferro-ferricyanide. When the sensor was exposed to 100 ng/mL of BPMV without any interfering virus, the DPV peak current decreased to 113 μA. However, when 100, 500, or 1000 ng/mL of SMV was added to 100 ng/mL of BPMV, there was only a slight change (RSD = 11.7%) in the DPV peak current compared to its response to the target BPMV alone (Figure 4a). The DPV peak current showed a low RSD of no more than 13.2% when the concentration of BPMV increased to 1000 ng/mL, and the concentration of SMV interferent remained the same (Figure 4b). This indicates that the sensor had considerable selectivity for BPMV in the presence of the interference virus.

The reproducibility of the sensors was assessed by measuring the same concentration of BPMV with four sensors that were produced using the same manufacturing process. The DPV responses of the four sensors to the PBS solution and 100 ng/mL BPMV were measured. The histogram displays the response peak currents of the four sensors tested (Figure 4c). The RSD of the mean DPV peak current was 7.5% for the baseline response and 9.2% for the response to 100 ng/mL BPMV, indicating considerable reproducibility of the sensor.

The sensor could be regenerated for multiple uses through a simple process of washing with acetic acid. This was demonstrated by exposing the sensor to a concentration of BPMV at 50 ng/mL. Following the completion of the DPV measurement, the surface of the sensor was cleaned with a 2%

https://doi.org/10.1021/acssensors.3c01478
ACS Sens. XXXX, XXX, XXX−XXX

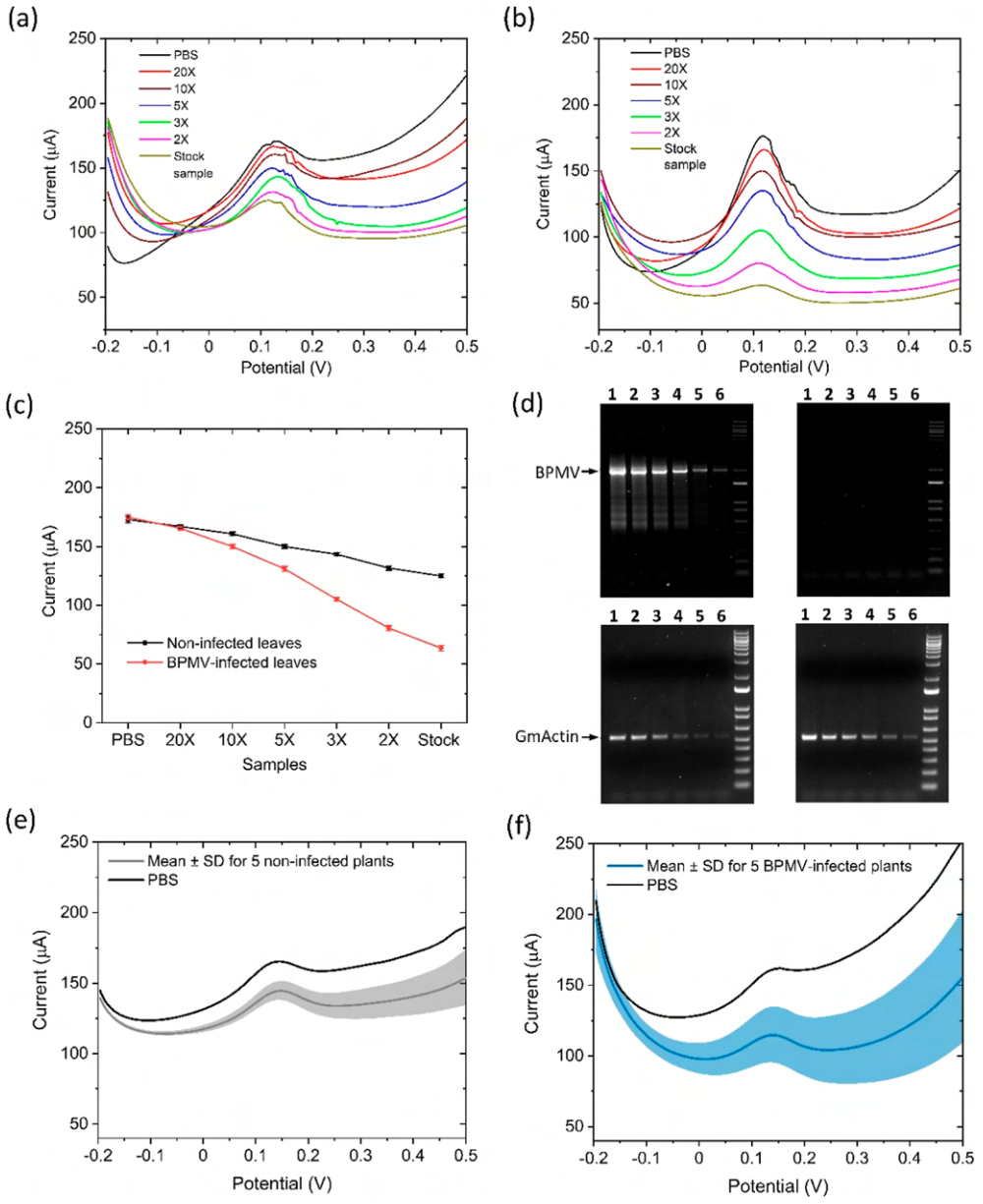

Figure 5. **(a,b)** DPV responses of the sensor to sequentially diluted noninfected leaf samples (a) and BPMV-infected leaf samples (b). (c) Comparison of the DPV responses of the sensor to serially diluted noninfected and BPMV-infected leaf samples. (d) RT-PCR was utilized to identify BPMV presence in leaf samples collected from both noninfected and BPMV-infected soybean plants. BPMV amplicon presence in BPMV-infected (top-left panel) and noninfected (top-right panel) leaves, with cDNA undergoing serial dilutions of 1800-, 3600-, 5400-, 9000-, 18,000-, and 36,000-fold, allocated to lanes 1−6 for BPMV detection. Internal control GmActin in BPMV-infected (bottom-left panel) and noninfected (bottom-right) leaves, where cDNA underwent serial dilutions of 10-, 20-, 30-, 50-, 100-, and 200-fold, assigned to lanes 1−6, respectively. (e,f) DPV responses for the sensor upon exposure to liquid samples obtained from five noninfected (e) and five BPMV-infected soybean plants (f). Liquid samples were extracted from all of the leaves of each individual plant. The shaded areas in (e,f) indicate the standard deviation of the measurements for five noninfected plants and five BPMV-infected ones, respectively.

v/v acetic acid solution for 10 min and then with DI water for an additional 5 min. The procedure effectively removed the entrapped BPMV particles within the Ppy polymer, hence restoring the active nanocavities. After the sensor was refreshed, a repeated cycle of BPMV detection and subsequent surface cleaning was implemented. Figure 4d shows that the sensor maintained a consistent DPV current response to the BPMV sample across the initial eight cycles; beyond this, a minor decline in the DPV current was observed, with an RSD of 6%, implying that the acetic acid wash presents a viable method for reactivating the nanocavities and reusing the sensor for multiple uses.

Table S1 presents a comparison of the analytical performance of the sensor for BPMV detection with previously reported methods.[6,50,55−58] Our sensor offers a broad dynamic detection range of 0.01−100,000 ng/mL, a low LOD of 41 pg/mL, and a short detection time of less than 2 min. These capabilities surpass those of other methods, making the sensor an appealing option for on-site BPMV testing due to its detection speed, high detectivity, cost effectiveness, and ease of use. Moreover, the sensor remained highly stable at room

https://doi.org/10.1021/acssensors.3c01478
ACS Sens. XXXX, XXX, XXX−XXX

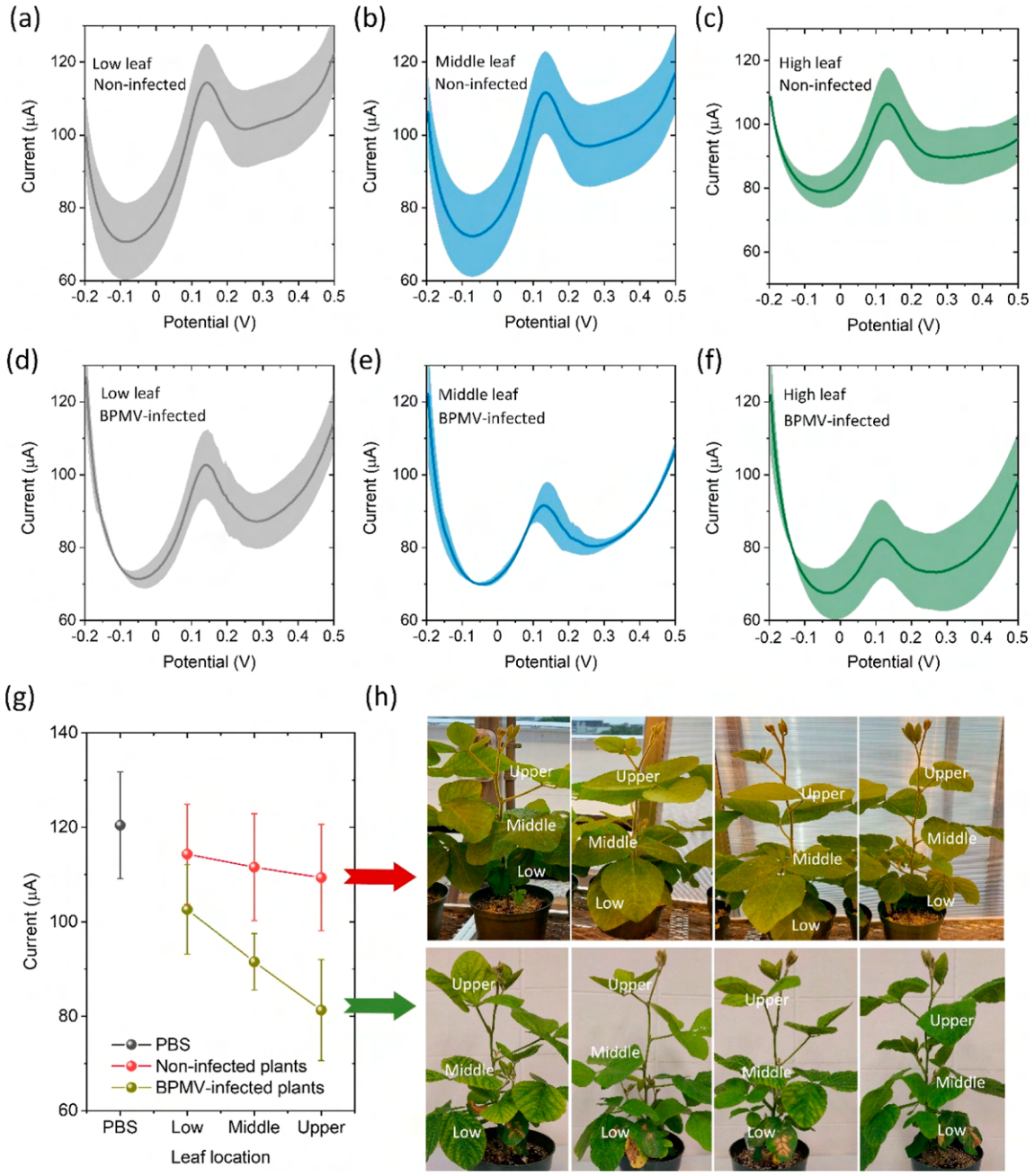

Figure 6. (a–f) DPV responses of the sensor to liquid samples extracted from the leaves at three distinct locations (low, middle, and upper) of both noninfected (a–c) and BPMV-infected soybean plants (d–f). The shaded area in parts (a–f) indicates the standard deviation of the measurements for five plants. (g) Comparison of DPV peak current output from the sensor in response to the PBS solution and liquid samples from noninfected and BPMV-infected soybean plants. (h) Images of noninfected (upper row) and BPMV-infected (lower row) soybean plants used in this study.

temperature during both storage and operation. The sensor also exhibits considerable selectivity toward the target virus compared to a nonspecific soybean virus and retains a strong binding capacity to the target virus even after washing with acetic acid. Notably, this study, to our knowledge, represents the pioneering endeavor to explore the potential of integrating MIP with an electrochemical transducer for the on-site detection of BPMV and can be used for the detection of other plant viruses.

Detection of BPMV in Leaves. Leaves were collected from both noninfected and BPMV-infected soybean plants in order to demonstrate the detection of BPMV in soybean leaves using the virus sensor without the need for sample preparation. Liquid was extracted from the collected leaves using a kitchen juice squeezer. The extracted liquid was serially diluted from 1×–20× fold in PBS containing 5 mM potassium ferro-ferricyanide.

The DPV measurement for the diluted samples of the noninfected leaves (Figure 5a) revealed that as the dilution ratio decreased from 20 to 0, the peak current decreased from 171 to 125 μA, which was attributed to nonspecific binding with the nanocavities formed on the sensor surface; however, the 27% change of the peak current was insignificant. In contrast, the DPV peak current for the diluted samples of the BPMV-infected leaves (Figure 5b) decreased significantly from 175 to 63 μA as the dilution ratio decreased from 20 to 0. This

https://doi.org/10.1021/acssensors.3c01478
ACS Sens. XXXX, XXX, XXX–XXX

is because the binding of BPMV particles to the nanocavities could cause an increase in electrochemical resistance, which would impede the diffusion of ferro-ferricyanide to the surface of the Au electrode. Figure 5c compares the DPV responses of the sensor to the serially diluted samples of noninfected and BPMV-infected leaves.

RT-PCR was employed to detect BPMV in leaf samples collected from both noninfected and BPMV-infected soybeans. The RT-PCR results were compared with the sensor's analytical performance (as shown in Figure 5a–d). For amplification of the internal control (GmActin), the cDNA was diluted by 10, 20, 30, 50, 100, and 200 fold, corresponding to lanes 1, 2, 3, 4, 5, and 6 for samples containing BPMV (Figure 5d). The RT-PCR amplicons for GmActin in the BPMV-infected leaf samples are shown in Figure 5d (bottom-left panel) and for the noninfected leaf samples (bottom-right). Because of the high abundance of BPMV, the cDNA was diluted by 1800, 3600, 5400, 9000, 18,000, and 36,000 folds, corresponding to lanes 1, 2, 3, 4, 5, and 6, respectively, for the detection of BPMV in infected leaf samples (Figure 5d; top-left panel) and for noninfected leaf samples (top-right panel). The RT-PCR analyses showed a distinct difference between the accumulation of the BPMV amplicon in BPMV-infected leaf samples versus the lack of the BPMV amplicon in noninfected leaf samples (Figure 5d), which is analytically consistent with the response of the sensor (as shown in Figure 5a,b). The presence of the internal GmActin control amplicons in BPMV-infected and noninfected samples demonstrates the specificity of the BPMV-specific PCR amplicon. These results validate the presence of BPMV in the infected leaf samples and further demonstrate that the sensor can be used as a technique for the specific detection of BPMV in soybean leaves.

To assess the analytical capabilities of the sensor, five noninfected soybean plants and five BPMV-infected plants were tested using the sensor (Figure 5e,f). Every leaf from each plant was collected, and liquid samples were obtained using a juice squeezer. For every sensor measurement, a 25 μL aliquot of the liquid sample extracted from the plant leaves was mixed with 75 μL of 10 mM PBS (pH 7.4) containing 5 mM potassium ferro-ferricyanide. Following this, 30 μL of the mixed sample was pipetted onto the sensor surface to carry out the DPV analysis. For the noninfected plants, the sensor displayed a minor decrease in DPV peak current from the baseline current, likely due to the nonspecific binding of interference molecules to the nanocavities on the sensor surface (Figure 5e). In contrast, the BPMV-infected plants demonstrated a significant change in the DPV peak current, presumably due to the specific binding of the virus to the nanocavities (Figure 5f). The observed data indicates a substantial variation between the infected plants with respect to the amount of BPMV present. These findings demonstrate the potential of the sensor to distinguish between the presence and absence of BPMV, as well as its ability to quantify the amount of virus present in an infected plant. These results support the possibility of using the sensor as a diagnostic tool for rapid, high-throughput detection of BPMV in soybean plants.

We examined the spatial variation of the BPMV concentration across different leaves of a soybean plant (Figure 6). To accomplish this, a cohort of four BPMV-infected plants and the other group of four noninfected plants were examined. The lowest leaf (primary leaf) was inoculated with BPMV or mock-inoculated at 14 days after sowing. After systemic infections occurred, liquid samples were extracted using a juice squeezer from three different leaves (namely low, middle, and upper leaves) from each plant after a period of 14 days postinfection. For each sensor measurement, 25 μL of the extracted sample was mixed with 75 μL of 10 mM PBS (pH 7.4); the mixed sample was loaded onto the sensor surface using a pipet. The corresponding DPV peak current for each sample from noninfected plants displayed a minor decrease with an increase in the height of the leaf location (Figure 6a–c), perhaps due to the nonspecific binding that occurred at the sensor surface. However, the current peak response for the liquid samples taken from the BPMV-infected plants revealed a considerable decrease from the baseline current. Furthermore, the peak current exhibited a decrease as the leaf location increased (Figure 6d–f), thereby indicating an increasing concentration of BPMV from the lower to the upper leaves. This observation suggested that the virus infection initiated at the lower leaves and propagated and accumulated to greater levels in the younger upper leaves, which is consistent with the expected distribution and accumulation of BPMV. Figure 6g shows a comparison between the current output of the sensor for the samples obtained from the noninfected and BPMV-infected soybean plants displayed in Figure 6h.

CONCLUSIONS

In summary, we have created a portable electrochemical biosensor for the rapid, selective, and sensitive detection of BPMV in soybean plants. The sensor technology represents a portable, on-site diagnostic solution for efficient virus detection in plants, circumventing complex and time-consuming sample treatment procedures. By employing MIP technology in conjunction with porous Ppy and an electrochemical transducer, the sensor surpasses conventional techniques such as ELISA and RT-PCR in terms of sensitivity, detection range, LOD, and response time. The sensor is capable of effectively differentiating BPMV-infected soybean plants from healthy ones and quantifying the virus concentrations, offering critical spatial data on the distribution of the virus across different leaves of a single plant. Owing to its ease of use, cost-effectiveness, high detectivity, and stability, this sensor technology is well-suited for on-site BPMV testing, eliminating the need for intricate and lengthy sample preparation processes. It is important to highlight the necessity for a comprehensive study of the interaction between imprinted nanocavities and BPMV. Potential future studies could delve into understanding the binding affinity and thermodynamics of these interactions, possibly using techniques such as molecular docking and molecular dynamics simulations. Also, the presented sensor technology could be further refined and adapted to detect other plant viruses or even extended to applications in human or animal health diagnostics. Additionally, integrating this sensor with wireless communication technology and many other recently developed plant, soil, and environmental sensors could enable real-time monitoring and data sharing, facilitating more effective disease,[59−61] nutrient,[62−64] and water[65−67] management and crop surveillance. This would ultimately contribute to the early detection and control of various plant diseases, significantly enhancing the health and productivity of crops.

https://doi.org/10.1021/acssensors.3c01478
ACS Sens. XXXX, XXX, XXX−XXX

■ ASSOCIATED CONTENT

Supporting Information

The Supporting Information is available free of charge at https://pubs.acs.org/doi/10.1021/acssensors.3c01478.

Electropolymerization of pyrrole with PBMV via chronoamperometry and comparison of BPMV detection performance between our sensor and literature-reported sensors (PDF)

■ AUTHOR INFORMATION

Corresponding Author

Liang Dong − *Department of Electrical and Computer Engineering, Iowa State University, Ames, Iowa 50011, United States; Microelectronics Research Center, Iowa State University, Ames, Iowa 50011, United States;* orcid.org/0000-0002-0967-4955; Phone: +1 (515) 294-0388; Email: ldong@iastate.edu

Authors

Nawab Singh − *Department of Electrical and Computer Engineering, Iowa State University, Ames, Iowa 50011, United States; Microelectronics Research Center, Iowa State University, Ames, Iowa 50011, United States*

Raufur Rahman Khan − *Department of Electrical and Computer Engineering, Iowa State University, Ames, Iowa 50011, United States; Microelectronics Research Center, Iowa State University, Ames, Iowa 50011, United States*

Weihui Xu − *Department of Plant Pathology, Entomology, and Microbiology, Iowa State University, Ames, Iowa 50011, United States*

Steven A. Whitham − *Department of Plant Pathology, Entomology, and Microbiology, Iowa State University, Ames, Iowa 50011, United States*

Complete contact information is available at: https://pubs.acs.org/10.1021/acssensors.3c01478

Author Contributions

N.S. designed and conducted the experiments. R.R.K. and N.S. fabricated the device and materials. W.X. prepared plant and virus samples and conducted RT-PCR tests. L.D. and S.A.W. conceived the sensor concept and supervised the research of N.S., R.R.K., and W.X. All authors analyzed the data. N.S. and L.D. drafted the manuscript. R.R.K., N.S., and S.A.W. provided inputs to the draft.

Notes

The authors declare no competing financial interest.

■ ACKNOWLEDGMENTS

This work was supported in part by the Iowa Soybean Research Center and the Plant Sciences Institute at Iowa State University; in part by the U.S. Department of Agriculture-National Institute of Food and Agriculture (USDA-NIFA) under grant numbers 2018-67021-27845, 2020-67021-31528, 2020-68013-30934, and Hatch Project 04308; in part by the U.S. National Science Foundation under grant numbers CNS-2125484 and IOS-1844563; and in part by the AI Research Institutes program supported by NSF and USDA-NIFA under AI Institute for Resilient Agriculture under grant number 2021-67021-35329.

■ REFERENCES

(1) Dhiman, S.; Yadav, A.; Debnath, N.; Das, S. Application of core/shell nanoparticles in smart farming: A paradigm shift for making the agriculture sector more sustainable. *J. Agric. Food Chem.* **2021**, *69* (11), 3267−3283.

(2) Misiou, O.; Koutsoumanis, K. Climate change and its implications for food safety and spoilage. *Trends Food Sci. Technol.* **2022**, *126*, 142−152.

(3) Savary, S.; Ficke, A.; Aubertot, J. N.; Hollier, C. Crop losses due to diseases and their implications for global food production losses and food security. *Food Secur.c* **2012**, *4* (4), 519−537.

(4) Khater, M.; de la Escosura-Muñiz, A.; Quesada-González, D.; Merkoçi, A. Electrochemical detection of plant virus using gold nanoparticle-modified electrodes. *Anal. Chim. Acta* **2019**, *1046*, 123−131.

(5) Hill, J. H.; Steven, A. W.. Control of virus diseases in soybeans. In *Advances in virus research*; Academic Press, 2014; Vol. *90*, pp 355−390.

(6) Giesler, L. J.; Ghabrial, S. A.; Hunt, T. E.; Hill, J. H. Bean pod mottle virus: a threat to US soybean production. *Plant Dis.* **2002**, *86* (12), 1280−1289.

(7) Yang, Q. Q.; Zhao, X. X.; Wang, D.; Zhang, P. J.; Hu, X. N.; Wei, S.; Liu, J. Y.; Ye, Z. H.; Yu, X. P. A reverse transcription-cross-priming amplification method with lateral flow dipstick assay for the rapid detection of Bean pod mottle virus. *Sci. Rep.* **2022**, *12* (1), 681−688.

(8) Bandara, A. Y.; Weerasooriya, D. K.; Bradley, C. A.; Allen, T. W.; Esker, P. D. Dissecting the economic impact of soybean diseases in the United States over two decades. *PLoS One* **2020**, *15* (4), No. e0231141.

(9) Zhou, J.; Tzanetakis, I. E. Soybean vein necrosis orthotospovirus can move systemically in soybean in the presence of bean pod mottle virus. *Virus Genes* **2020**, *56*, 104−107.

(10) Gu, H.; Clark, A. J.; De Sa, P. B.; Pfeiffer, T. W.; Tolin, S.; Ghabrial, S. A. Diversity among isolates of Bean pod mottle virus. *Phytopathology* **2002**, *92*, 446−452.

(11) Hobbs, H. A.; Hartman, G. L.; Wang, Y.; Hill, C. B.; Bernard, R. L.; Pedersen, W. L.; Domier, L. L. Occurrence of seed coat mottling in soybean plants inoculated with Bean pod mottle virus and Soybean mosaic virus. *Plant Dis.* **2003**, *87*, 1333−1336.

(12) Ross, J. P. Response of early-and late-planted soybeans to natural infection by bean pod mottle virus. *Plant Dis.* **1986**, *70* (3), 222−224.

(13) Shahraeen, N.; Ghotbi, T.; Salati, M.; Sahandi, A. First report of Bean pod mottle virus in soybean in Iran. *Plant Dis.* **2005**, *89* (7), 775.

(14) Fribourg, C. E.; Perez, W. Bean pod mottle virus (BPMV) affecting Glycine max (L.) Merr. in the Peruvian jungle. *Fitopatologia* **1994**, *29* (3), 207−210.

(15) Michelutti, R.; Tu, J. C.; Hunt, D. W. A.; Gagnier, D.; Anderson, T. R.; Welacky, T. W.; Tenuta, A. U. First report of Bean pod mottle virus in soybean in Canada. *Plant Dis.* **2002**, *86* (3), 330.

(16) Fulton, J.; Cumberland, D.; Hodgsen, O.; Amsoy, C.; Vickery, W. Bean pod mottle virus: occurrence in Nebraska and seed transmission in soybeans. *Plant Dis.* **1983**, *67*, 230−233.

(17) Anjos, J. R. N.; Brioso, P. S. T.; Charchar, M. J. A. Partial characterization of bean pod mottle virus in soyabeans in Brazil. *Fitopatol. Bras.* **1999**, *24* (1), 85−87.

(18) Ali, A. Rapid detection of fifteen known soybean viruses by dot-immunobinding assay. *J. Virol. Methods* **2017**, *249*, 126−129.

(19) Meisheng, W.; Ning, X.; Chunquan, Z.; Ghabrial, S. A. Detection of Bean pod mottle virus by RT-PCR. *Soybean Sci.* **2005**, *24* (4), 317−319.

(20) Shen, J. G.; Wang, N. W.; Gao, F. L.; Huang, K. H.; Guo, Q. X. Detection of Bean pod mottle virus by one-step IC-RT-PCR. *Chin. Agric. Sci. Bull.* **2009**, *25* (1), 176−179.

(21) Wen, W. G.; Cui, J. X.; Zhao, X. L.; Xu, Y.; Chen, X. F. Detection of Bean pod mottle virus by semi-nested RT-PCR in imported soybean. *Acta Phytopathol. Sin.* **2006**, *36* (4), 296−300.

(22) Shen, J.; Gao, F. L.; Cai, W. Multiplex RT-PCR for simultaneous detection of Bean pod mottle virus and Soybean mosaic

virus in imported soybean seeds. *Sci. Agric. Sin.* **2016**, *49* (4), 667−676.
(23) Hong, S.; Lee, C. The current status and future outlook of quantum dot-based biosensors for plant virus detection. *Plant Pathol. J.* **2018**, *34* (2), 85−92.
(24) Rafidah, A.; Faridah, S.; Shahrul, A. A.; Mazidah, M.; Zamri, I. Chronoamperometry measurement for rapid cucumber mosaic virus detection in plants. *Procedia Chem.* **2016**, *20*, 25−28.
(25) Zhang, Y.; Li, P.; Hou, M.; Chen, L.; Wang, J.; Yang, H.; Feng, W. An electrochemical biosensor based on ARGET ATRP with DSN-assisted target recycling for sensitive detection of tobacco mosaic virus RNA. *Bioelectrochemistry* **2022**, *144*, 108037.
(26) Amouzadeh Tabrizi, M.; Fernández-Blázquez, J. P.; Medina, D. M.; Acedo, P. An ultrasensitive molecularly imprinted polymer-based electrochemical sensor for the determination of SARS-CoV-2-RBD by using macroporous gold screen-printed electrode. *Biosens. Bioelectron.* **2022**, *196*, 113729.
(27) Raziq, A.; Kidakova, A.; Boroznjak, R.; Reut, J.; Öpik, A.; Syritski, V. Development of a portable MIP-based electrochemical sensor for detection of SARS-CoV-2 antigen. *Biosens. Bioelectron.* **2021**, *178*, 113029.
(28) Karimian, N.; Vagin, M.; Zavar, M. H. A.; Chamsaz, M.; Turner, A. P.; Tiwari, A. An ultrasensitive molecularly-imprinted human cardiac troponin sensor. *Biosens. Bioelectron.* **2013**, *50*, 492−498.
(29) Jolly, P.; Tamboli, V.; Harniman, R. L.; Estrela, P.; Allender, C. J.; Bowen, J. L. Aptamer−MIP hybrid receptor for highly sensitive electrochemical detection of prostate specific antigen. *Biosens. Bioelectron.* **2016**, *75*, 188−195.
(30) Wang, Y.; Zhang, Z.; Jain, V.; Yi, J.; Mueller, S.; Sokolov, J.; Liu, Z.; Levon, K.; Rigas, B.; Rafailovich, M. H. Potentiometric sensors based on surface molecular imprinting: Detection of cancer biomarkers and viruses. *Sens. Actuators, B* **2010**, *146* (1), 381−387.
(31) Bolisay, L. D.; Culver, J. N.; Kofinas, P. Molecularly imprinted polymers for tobacco mosaic virus recognition. *Biomaterials* **2006**, *27* (22), 4165−4168.
(32) Dickert, F. L.; Hayden, O.; Bindeus, R.; Mann, K. J.; Blaas, D.; Waigmann, E. Bioimprinted QCM sensors for virus detection—screening of plant sap. *Anal. Bioanal. Chem.* **2004**, *378* (8), 1929−1934.
(33) Jamalipour Soufi, G.; Iravani, S.; Varma, R. S. Molecularly imprinted polymers for the detection of viruses: Challenges and opportunities. *Analyst* **2021**, *146* (10), 3087−3100.
(34) Khan, R. R.; Ibrahim, H.; Rawal, G.; Zhang, J.; Lu, M.; Dong, L. Multichannel microfluidic virus sensor for rapid detection of respiratory viruses using virus-imprinted polymer for digital livestock farming. *Sens. Actuators, B* **2023**, *389*, 133920.
(35) Lowdon, J. W.; Diliën, H.; Singla, P.; Peeters, M.; Cleij, T. J.; van Grinsven, B.; Eersels, K. MIPs for commercial application in low-cost sensors and assays−An overview of the current status quo. *Sens. Actuators, B* **2020**, *325*, 128973.
(36) Karimian, N.; Hashemi, P.; Khanmohammadi, A.; Afkhami, A.; Bagheri, H. The principles and recent applications of bioelectrocatalysis. *Anal. Bioanal. Chem. Res.* **2020**, *7* (3), 281−301.
(37) Wang, L.; Wang, H.; Tang, X.; Zhao, L. Molecularly imprinted polymers-based novel optical biosensor for the detection of cancer marker lysozyme. *Sens. Actuators, A* **2022**, *334*, 113324.
(38) Ali, M. A.; Dong, L.; Dhau, J.; Khosla, A.; Kaushik, A. Perspective—electrochemical sensors for soil quality assessment. *J. Electrochem. Soc.* **2020**, *167* (3), 037550.
(39) Ali, M. A.; Jiang, H.; Mahal, N. K.; Weber, R. J.; Kumar, R.; Castellano, M. J.; Dong, L. Microfluidic impedimetric sensor for soil nitrate detection using graphene oxide and conductive nanofibers enabled sensing interface. *Sens. Actuators, B* **2017**, *239*, 1289−1299.
(40) Singh, N.; Ali, M. A.; Suresh, K.; Agrawal, V. V.; Rai, P.; Sharma, A.; Malhotra, B.; John, R. In-situ electrosynthesized nanostructured Mn3O4-polyaniline nanofibers-biointerface for endocrine disrupting chemical detection. *Sens. Actuators, B* **2016**, *236*, 781−793.
(41) Ren, S.; Cui, W.; Liu, Y.; Cheng, S.; Wang, Q.; Feng, R.; Zheng, Z. Molecularly imprinted sensor based on 1T/2H MoS2 and MWCNTs for voltammetric detection of acetaminophen. *Sens. Actuators, A* **2022**, *345*, 113772.
(42) AL-Ammari, R. H.; Ganash, A. A.; Salam, M. A. Electrochemical molecularly imprinted polymer based on zinc oxide/graphene/poly (o-phenylenediamine) for 4-chlorophenol detection. *Synth. Met.* **2019**, *254*, 141−152.
(43) Regasa, M. B.; Refera Soreta, T.; Femi, O. E.; C Ramamurthy, P. Development of molecularly imprinted conducting polymer composite film-based electrochemical sensor for melamine detection in infant formula. *ACS Omega* **2020**, *5* (8), 4090−4099.
(44) Pardieu, E.; Cheap, H.; Vedrine, C.; Lazerges, M.; Lattach, Y.; Garnier, F.; Remita, S.; Pernelle, C. Molecularly imprinted conducting polymer based electrochemical sensor for detection of atrazine. *Anal. Chim. Acta* **2009**, *649* (2), 236−245.
(45) Kim, S.; Jang, L. K.; Park, H. S.; Lee, J. Y. Electrochemical deposition of conductive and adhesive polypyrrole-dopamine films. *Sci. Rep.* **2016**, *6* (1), 30475−30478.
(46) Dakshayini, B. S.; Reddy, K. R.; Mishra, A.; Shetti, N. P.; Malode, S. J.; Basu, S.; Naveen, S.; Raghu, A. V. Role of conducting polymer and metal oxide-based hybrids for applications in ampereometric sensors and biosensors. *Microchem. J.* **2019**, *147*, 7−24.
(47) Ratautaite, V.; Boguzaite, R.; Brazys, E.; Ramanaviciene, A.; Ciplys, E.; Juozapaitis, M.; Slibinskas, R.; Bechelany, M.; Ramanavicius, A. Molecularly imprinted polypyrrole based sensor for the detection of SARS-CoV-2 spike glycoprotein. *Electrochim. Acta* **2022**, *403*, 139581.
(48) Wu, Y.; Li, G.; Tian, Y.; Feng, J.; Xiao, J.; Liu, J.; Liu, X.; He, Q. Electropolymerization of molecularly imprinted polypyrrole film on multiwalled carbon nanotube surface for highly selective and stable determination of carcinogenic amaranth. *J. Electroanal. Chem.* **2021**, *895*, 115494.
(49) Lu, G.; Li, C.; Shi, G. Polypyrrole micro-and nanowires synthesized by electrochemical polymerization of pyrrole in the aqueous solutions of pyrenesulfonic acid. *Polymer* **2006**, *47* (6), 1778−1784.
(50) Blinova, N. V.; Stejskal, J.; Trchová, M.; Prokeš, J.; Omastová, M. Polyaniline and polypyrrole: A comparative study of the preparation. *Eur. Polym. J.* **2007**, *43* (6), 2331−2341.
(51) Li, T.; Chen, Z.; Johnson, J. E.; Thomas, G. J. Structural studies of bean pod mottle virus, capsid and RNA in crystal and solution states by laser Raman spectroscopy. *Biochemistry* **1990**, *29* (21), 5018−5026.
(52) Li, T.; Chen, Z.; Johnson, J. E.; Thomas, G. J. Conformations, interactions, and thermostabilities of RNA and proteins in bean pod mottle virus: investigation of solution and crystal structures by laser Raman spectroscopy. *Biochemistry* **1992**, *31* (29), 6673−6682.
(53) Renugopalakrishnan, V.; Piazzolla, P.; Tamburro, A. M.; Lamba, O. P. Structural studies of cucumber mosaic virus: Fourier transform infrared spectroscopic studies. *IUBMB Life* **1998**, *46* (4), 747−754.
(54) Çakıroğlu, B.; Jabiyeva, N.; Holzinger, M. Photosystem II as a chemiluminescence-induced photosensitizer for photoelectrochemical biofuel cell-type biosensing system. *Biosens. Bioelectron.* **2023**, *226*, 115133.
(55) Zhang, M.; Chen, W.; Chen, X.; Zhang, Y.; Lin, X.; Wu, Z.; Li, M. Multiplex immunoassays of plant viruses based on functionalized upconversion nanoparticles coupled with immunomagnetic separation. *J. Nanomater.* **2013**, *2013*, 317437.
(56) McClellan, M. S.; Domier, L. L.; Bailey, R. C. Label-free virus detection using silicon photonic microring resonators. *Biosens. Bioelectron.* **2012**, *31* (1), 388−392.
(57) Ghabrial, S. A.; Schultz, F. Serological Detection of Bean Pod Mottle Virus in Bean Leaf Beetles. *Phytopathology* **1983**, *73* (3), 480−483.
(58) Liao, F.; Guo, J.; Liu, P.; Zhang, Y.; Huang, G. Detection of Bean pod mottle virus in soybean by one step assay of RT-PCR and

https://doi.org/10.1021/acssensors.3c01478
ACS Sens. XXXX, XXX, XXX−XXX

real-time fluorescent RT-PCR. *Acta Phytophylacica Sin.* **2009**, *36* (2), 141−145.
(59) Ibrahim, H.; Moru, S.; Schnable, P.; Dong, L. Wearable Plant Sensor for In Situ Monitoring of Volatile Organic Compound Emissions from Crops. *ACS Sens.* **2022**, *7* (8), 2293−2302.
(60) Tabassum, S.; Kumar, R.; Dong, L. Plasmonic crystal-based gas sensor toward an optical nose design. *IEEE Sens. J.* **2017**, *17* (19), 6210−6223.
(61) Li, Z.; Paul, R.; Ba Tis, T.; Saville, A. C.; Hansel, J. C.; Yu, T.; Ristaino, J. B.; Wei, Q. Non-invasive plant disease diagnostics enabled by smartphone-based fingerprinting of leaf volatiles. *Nat. Plants* **2019**, *5* (8), 856−866.
(62) Ibrahim, H.; Yin, S.; Moru, S.; Zhu, Y.; Castellano, M. J.; Dong, L. In Planta Nitrate Sensor Using a Photosensitive Epoxy Bioresin. *ACS Appl. Mater. Interfaces* **2022**, *14* (22), 25949−25961.
(63) Chen, Y.; Tang, Z.; Zhu, Y.; Castellano, M. J.; Dong, L. Miniature multi-ion sensor integrated with artificial neural network. *IEEE Sens. J.* **2021**, *21* (22), 25606−25615.
(64) Zhu, Y.; Chen, Y.; Ali, M. A.; Dong, L.; Wang, X.; Archontoulis, S. V.; Schnable, J. C.; Castellano, M. J. Continuous in situ soil nitrate sensors: the importance of high-resolution measurements across time and a comparison with salt extraction-based methods. *Soil Sci. Soc. Am. J.* **2021**, *85* (3), 677−690.
(65) Yin, S.; Ibrahim, H.; Schnable, P. S.; Castellano, M. J.; Dong, L. A Field-Deployable, Wearable Leaf Sensor for Continuous Monitoring of Vapor-Pressure Deficit. *Adv. Mater. Technol.* **2021**, *6* (6), 2001246.
(66) Chen, Y.; Tian, Y.; Wang, X.; Wei, L.; Dong, L. Miniaturized, Field-Deployable, Continuous Soil Water Potential Sensor. *IEEE Sens. J.* **2020**, *20* (23), 14109−14117.
(67) Black, W. L.; Santiago, M.; Zhu, S.; Stroock, A. D. Ex situ and in situ measurement of water activity with a MEMS tensiometer. *Anal. Chem.* **2020**, *92* (1), 716−723.

https://doi.org/10.1021/acssensors.3c01478
ACS Sens. XXXX, XXX, XXX−XXX